JACS
JOURNAL OF THE AMERICAN CHEMICAL SOCIETY

COMMUNICATION

pubs.acs.org/JACS

Self-Assembled Hollow Nanospheres Strongly Enhance Photoluminescence

Damei Ke,[†] Chuanlang Zhan,[*,†] Shuangping Xu,[‡] Xunlei Ding,[§] Aidong Peng,[†] Jin Sun,[‡] Shenggui He,[§] Alexander D. Q. Li,[*,¶] and Jiannian Yao[*,†]

[†]Laboratory of Photochemistry and [§]State Key Laboratory for Structural Chemistry of Unstable and Stable Species, Beijing National Laboratory for Molecular Sciences, Institute of Chemistry, Chinese Academy of Sciences, Beijing 100190, P. R. China

[‡]Institute of Polymer Materials, Qingdao University, Qingdao 266071, P. R. China

[¶]Department of Chemistry, Washington State University, Pullman, Washington 99164, United States

Supporting Information

ABSTRACT: We report that two molecular building blocks differ only by two protons, yet they form totally different nanostructures. The protonated one self-organized into hollow nanospheres (~200 nm), whereas the one without the protons self-assembled into rectangular plates. Consequently, the geometrically defined nanoassemblies exhibit radically different properties. As self-assembly directing units, protons impart ion-pairing and hydrogen-bonding probabilities. The plate-forming nanosystem fluoresces weakly, probably due to energy transfer among chromophores ($\Phi < 0.2$), but the nanospheres emit strong yellow fluorescence ($\Phi \approx 0.58-0.85$).

Large planar π-aromatic compounds such as perylene diimides (PDIs), porphyrins, and phthalocyanines possess a strong propensity to form end-opened 1-D self-assemblies.[1−3] Amphiphilic molecules, however, can form not only end-opened membrane-like structures but also hollow and spherical nanostructures such as vesicles.[4] Until now, molecules have been designed using intrinsic curvature to impart spherical or sphere-like structures.[5] These examples included (1) U-shaped[5a,b] or double-decker units,[5c] (2) wedge- and dumbbell-shaped molecules,[5d,e] and (3) metal-coordination-induced bending.[5f] In fact, molecular shapes determine the final self-assembled morphologies of these nanostructures. Alternatively, we seek to use intermolecular interactions to control nanomorphology. The specific question to be addressed is how to control the secondary interactions of large, rigid π-aromatic dyes so that they self-organize into hollow nanospheres.

Herein, we use PDI derivatives to illustrate this principle. The 1- and 7-positions of PDI dyes can be easily modified using a wide range of functional groups.[1,2,6] In particular, we introduced two pyridyl groups at the 1- and 7-positions of PDI dyes and utilized the protonation ability of the pyridine to tune the intermolecular interactions of charge pairing and hydrogen bonding. The unprotonated 1,7-bispyridyloxy perylene diimide (**1**) has neither charges nor hydrogen bond donors. Therefore, its major secondary interactions are solvophobic and dipole−dipole interactions. The protonated 1,7-bispyridyloxy perylene diimide (**2**) gains both charge-pairing and hydrogen-bonding forces in addition to solvophobic and dipolar interactions (Scheme 1). As a result, dye **1** formed into weakly fluorescent plates, whereas dye **2** assembled into highly fluorescent hollow nanospheres.

Scheme 1. (a) Chemical Structures of Dyes 1−4, (b) Plate-like Structures, in Which π-Stacking among Chromophores Causes Fluorescence Quenching, and (c) Hollow Nanospheres Formed as a Result of Introducing Charge Interactions and Hydrogen Bonding[a]

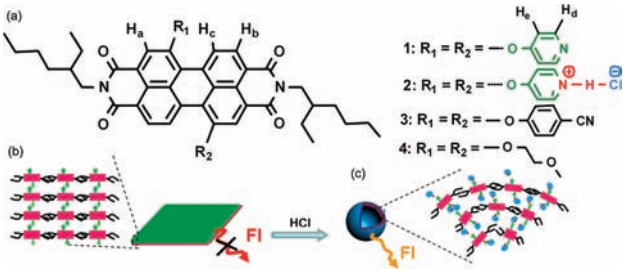

[a] Because the chromophores do not rely on stacking interactions only, strong fluorescence enhancement was observed.

Addition of excess hydrochloric acid (12 M) completely protonated dye **1**. This protonation was confirmed by an obvious red-to-orange color change and well-resolved vibronic splitting (Supporting Information, Figure S1). As controls, compounds **3** and **4** were synthesized, but neither color change nor vibronic splitting was significantly altered by addition of hydrochloric acid (Figures S2 and S3).

Morphological studies revealed dye **2** forms hollow nanospheres like micelles (Figure 1a). As concentration increased in methanol (MeOH), the sizes of hollow nanospheres also expanded, from 50 to 200 nm in Figure 1b (1×10^{-6} M) and c (1×10^{-4} M) to 200−300 nm in Figure 1d (1×10^{-3} M) and 400−600 nm in Figure 1e (1×10^{-2} M). Dynamic light scattering (DLS) confirmed the formation of nanospheres in the solution (Figure S4). Interestingly, a number of nanospheres formed fused structures at high concentration levels, but the hollow and spherical nature was well preserved, and no collapsed morphologies were observed (Figure 1e). In less polar solvents such as ethanol (EtOH), acetone, and ethyl acetate (EtOAc), dye

Received: March 9, 2011
Published: June 23, 2011

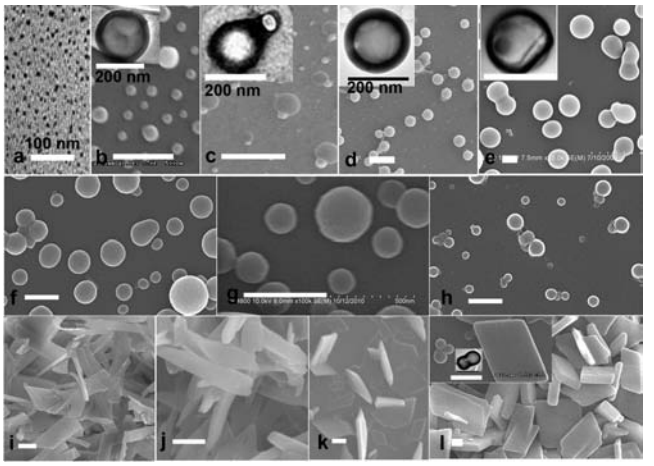

Figure 1. SEM and TEM (inset) images of the spherical micelles formed from **2** at 6×10^{-7} M (a) and hollow nanospheres formed at 1×10^{-6} (b), 1×10^{-4} (c), 1×10^{-3} (d), and 1×10^{-2} M (e) in MeOH. SEM images of the hollow nanospheres formed from **2** in 1×10^{-3} M EtOH (f), 1×10^{-3} M acetone (g), and 1×10^{-4} M EtOAc (h). SEM and TEM (inset) images of the plate structures formed from **1** in 1×10^{-4} M EtOAc (i), 1×10^{-3} M acetone (j), 1×10^{-3} M EtOH (k), and 1×10^{-3} M MeOH (l). The unlabeled scale bars represent 500 nm.

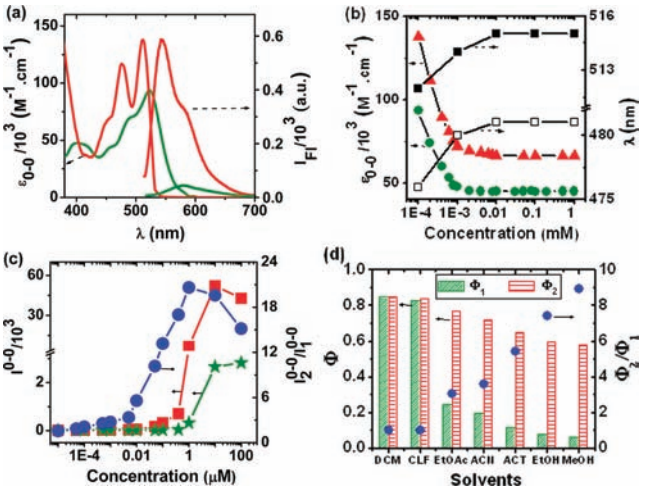

Figure 2. (a) Absorption and fluorescence spectra of **2** (red lines) and **1** (green lines) in MeOH at [dye] = 1×10^{-7} M. (b) Concentration-dependent ε_{0-0} values for **2** (red triangles) and **1** (green circles) as well as $\lambda_{max}^{a,0-0}$ (black squares) and $\lambda_{max}^{a,0-1}$ (open squares) of **2**. (c) Concentration-dependent fluorescent intensity (I^{0-0}) of **2** (red squares) and **1** (green stars) and I_2^{0-0}/I_1^{0-0} ratio of the two dyes (blue circles). (d) Fluorescent quantum yield (Φ) of **2** (red bars) and **1** (green bars) in different solvents ([dye] = 1×10^{-6} M). The blue circles represent the Φ_2/Φ_1 values in different solvents using excitation wavelength λ_{Ex} = 490 nm. Abbreviations in (d): DCM, dichloromethane; CLF, chloroform; ACN, acetonitrile; and ACT, acetone.

2 at high concentrations always formed hollow nanospheres (Figure 1f–h). Many fused spheres were observed from these solvents, but no collapsed morphologies. These results strongly suggest that the hollow nanospheres are highly stable as the concentration or solvent polarity changes.

In striking contrast, the self-assembled morphologies of dye **1** strongly favor plate-like structures. In less polar solvents such as EtOAc, acetone, and EtOH, dye **1** always formed plate-like microstructures regardless of solvent polarity and dye concentration (Figure 1i–k). In methanol, the self-assembly of dye **1** underwent a phase transition from nanospheres (Figure S5) to rhombic microplates (Figures 1l and S6) as the concentration of **1** was increased from 1×10^{-4} to 1×10^{-3} M. The coexistence of microplates with a small quantity of hollow nanospheres supports the fact that the phase transition has occurred.

These morphological comparisons clearly demonstrate that protonation strongly favors not only the formation of hollow nanospheres but also their stability at higher concentrations and in different solvents. Therefore, the curvature driving forces for spherical self-organization are mostly charge pairing and hydrogen bonding, which operate in dye **2** intermolecularly but not in dye **1**. Such balanced interactions in dye **2** not only created hollow nanospheres but also maintained the spherical morphologies from collapsing under high concentrations or in less polar solvents.

Spectroscopic experiments were further conducted to gain insightful information about the self-assemblies of dyes **1** and **2**. The salient feature is that protonation of the pyridyl groups imparts totally different absorption and fluorescence spectra (Figure 2a). First, the protonated dye **2** absorbs 1.5 times more strongly than the unprotonated dye **1**, indicating an increase in the oscillator strength for the $S_0 \rightarrow S_1$ transition. Concomitantly, the pyridine $\pi \rightarrow \pi^*$ absorption, appearing at 300–400 nm, characterizes the formation of pyridinium cations (Figure S7).[7] Second, the lowest absorption band, the electronic $S_0 \rightarrow S_1$ transition, blue-shifted approximately $\Delta\lambda_{max}^{a,0-0}$ = 12 nm from 524 to 512 nm, hinting that dye **2** is more planar than dye **1**. Third, the protonated dye **2** has a well-resolved vibronic fine structure for the electronic $S_0 \rightarrow S_1$ transition when compared with the unprotonated dye **1**, again hinting that dye **2** is more planar than dye **1**. Fourth, the full width at half-maximum (fwhm) decreases from 3064.6 cm^{-1} for dye **1** to 2930.4 cm^{-1} for dye **2**, which further supports that the perylene core becomes more planar upon protonation of pyridyl groups.

The change in molecular conformations is caused by charge delocalization between pyridinium cations and perylene core. As revealed by quantum chemical calculations, the total Mulliken charge-density[8] (Table S1) delocalized on the perylene core increases from 0.36 to 0.60 as the pyridyl groups are protonated. Simultaneously, the negative charge-density distributed on the bridged oxygen atoms decreases from −0.76 to −0.68. The charge delocalization abates the dihedral angle between the two naphthalene rings by ∼0.85° (Table S2, Figure S8a,b).

The distinct features in fluorescent properties (also see Figures S1 and S9) include (i) dramatic enhancement of the fluorescent intensity; (ii) large blue-shift of the fluorescent band with $\Delta\lambda_{max}^{f,0-0}$ = 36 nm, from 578 to 542 nm; (iii) a much smaller Stokes's shift (1081 vs 1746 cm^{-1}); and (iv) a well-resolved vibronic fine structure with a shoulder around 578 nm for dye **2**. These results are consistent with the interpretation presented for absorption data.

The extinction coefficients ε_{0-0} in Figure 2b reveal that both dyes **1** and **2** possess a strong propensity to self-assemble in MeOH. Rather than being independent of concentration, the extinction coefficients violate Beer's law, decreasing through an inflection point at 1×10^{-6} M and transitioning to a plateau region, where Beer's law is obeyed. The plateau suggests maturation of self-assembly, such as reaching a critical size, consistent with the morphological observations. These plateaus are also echoed by the $\lambda_{max}^{a,0-0}$ and $\lambda_{max}^{a,0-1}$, both bathochromically

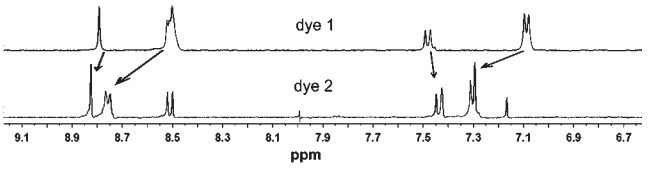

Figure 3. Partial NMR spectra of dye **1** (top) and dye **2** (bottom, [HCl] = 0.72 M) in CD_3OH: both samples contain 5.6 mM dye. DLS reveals that some nanostructures already form in solution because of strong light scattering. TEM and SEM further confirm that the nanostructures are nanoplates and nanospheres, respectively (see Figure 1).

shifted slightly from 512 to 515 nm and from 476 to 481 nm (Figure 2b), respectively. Upon self-assembly, the fwhm of the $S_0 \rightarrow S_1$ transition band between the nanospheres of dye **2** and plate-like structures of dye **1** also changes slightly. For example, at 1×10^{-3} M, the fwhm is 2532.2 cm^{-1} for dye **1** and 2476.8 cm^{-1} for dye **2**. This small variation indicates that only subtle alternation of the perylene $\pi-\pi$ packing occurs, accompanying the protonation, as the perylene cores adopt a more planar conformation.

Figure 2c displays that dye **2** always emits stronger fluorescence than dye **1** as the concentration of dye increases. Accordingly, the relative intensity of I_2^{0-0}/I_1^{0-0} increased from ~1.5 to 20.6 as the concentration was augmented from 10 pM to 1 μM. At the 1 μM concentration, the I_2^{0-0}/I_1^{0-0} ratio reaches the maximum, and fluorescence quantum yield of **2** (Φ_2) is 8.8 times larger than that of **1** (Φ_1). As concentration was further changed from 1 μM to 1 mM, the quantum yield ratio remained high, Φ_2/Φ_1 = 8.4−4.0 (Table S3). Both dyes **1** and **2** aggregated, but the nanospherical assemblies of dye **2** enhanced fluorescence ($\Phi_2 \leq$ 0.58 in MeOH only), while the plate-like assemblies of dye **1** quenched fluorescence ($\Phi_1 \leq$ 0.065 in MeOH only).

Solvent-dependent quantum yields reveal that the nanoplate assemblies dramatically quenched the fluorescence of **1**. In contrast, nanospherical assemblies hardly quenched the fluorescence of **2**. In good solvents such as chloroform or methylene chloride, both dyes **1** and **2** exist as free molecules rather than assemblies and thus have excellent quantum yields, $\Phi_1 = \Phi_2$ = 0.86 (Figure 2d). Poor solvents like acetone and EtOH drive the self-organization of both dyes, **1** into nanoplates and **2** into nanospheres. As **1** self-assembled into nanoplates, its quantum yield plummeted from Φ_1 = 0.86 to 0.065. When **2** self-assembled into nanospheres, however, its quantum yields did not change much, from Φ_2 = 0.86 to 0.58. Although most assemblies impart low quantum yields, an effect similar to concentration quenching, the results presented here are significant because together they prove that some self-assemblies can maintain excellent quantum yields.

NMR also confirms that perylene packing underwent only subtle changes upon protonation. As revealed by NMR spectra, protonation causes a large downfield shift of the pyridine H_d and H_e, respectively, from ~8.50 to 8.77 ppm and from 7.08 to 7.31 ppm. However, the doublet perylene aromatic protons H_c and H_b shift only slightly, from 7.48 to 7.45 ppm and from ~8.50 to 8.52 ppm, respectively. Similarly, the singlet perylene proton H_a also shifts slightly from 8.78 to 8.82 ppm (Figure 3). The small shifts of perylene proton resonance indicate that perylene packing is only slightly altered upon protonation. Mulliken charge-density calculations (Table S1) have validated the NMR results. Specifically, positive charge distribution of the aromatic hydrogen atoms increases by an average of +0.071 for pyridine-H_d, +0.061 for pyridine-H_e, +0.004 for perylene-H_a, and +0.016 for perylene-H_b, whereas it decreases by −0.010 for perylene-H_c (Table S4). All aromatic protons except perylene-H_c shift downfield due to lack of shielding. Participation of the pyridine units in the molecular HOMO decreases upon prontonation, whereas involvement of the LUMO increases upon protonation (Figure S8c,d). Thus, calculations agree with NMR data, and together they are consistent with absorption and fluorescence results.

The fluorescence enhancement of nanospheres over the nanoplates can be attributed to electronic effects and steric packing effects. Typically, introduction of electron-withdrawing groups at the 1,6,7,12-positions of PDIs improves fluorescence. For example, 1,6,7,12-tetrachloroperylene has a high fluorescence quantum yield,[9a] whereas amino substitution at these positions results in low quantum yields.[9b] Additionally, bulky steric hindrance, like in 1,6,7,12-tetraphenoxyperylene, prevents possible electron and energy transfer among perylene cores, thus enhancing quantum yields.[10] Here, the pyridinium units both functioned as electron-withdrawing groups and created large separation between perylene cores because positive charges repelled each other. Thus, both the steric effects and the electronic effects synergistically contribute to higher quantum yields of assemblies of **2**, but not **1**.

FT-IR measurements were further carried out to support hydrogen-bonding (H-bonds) contribution and solvent involvement in the nanostructures. First, perylene and pyridine C═C, C═N stretching in the region of 1800−1200 cm^{-1}, C−O stretching at 1200 cm^{-1}, and aromatic ring vibrations and C−H deformation in the region of 1150−400 cm^{-1} (Figures S10 and S11, Table S5) all shift slightly upon protonation. These small shifts are consistent with delocalization of the pyridinium charge. Second, H-bonds are involved in the hollow nanospheres, but not in the nanoplates. In particular, the vibration at 2440 cm^{-1} with medium intensity demonstrates formation of hydrogen-bonding of N−H···Cl^- from pyridinium chlorides in the nanosphere samples.[11a] The same conclusion is also confirmed by the hydrogen-bonding out-of-plane γ_{N-H} deformation mode at 1013 cm^{-1}.[11b] The broad and strong vibration band around 3400 cm^{-1} reveals hydrogen-bonded water and/or methanol trapped inside the nanospheres. In addition, the vibrations in the region of 2450−2800 cm^{-1} also evidence the hydrogen-bonding of N−H···Cl^-, N−H···OH, or O−H···Cl^- in the nanospheres.[11c] Third, the nanosphere samples had a strong vibration band at 1024 cm^{-1}, assigned to the C−O stretching in methanol, whereas nanoplate samples had no such band. Furthermore, the antisymmetric bending vibrations of CH_3 groups at 1440 cm^{-1} grew much stronger from nanoplates to nanospheres. Both of these observations indicate that methanol solvent was involved in the formation of nanospheres but not nanoplates.

The counterion effect was also examined. In addition to hydrochloric acid, concentrated hydrobromic acid (HBr, 8.3 M) and hydroiodic acid (HI, 7.4 M) were also used; SEM and DLS confirmed that both acids induced nanosphere formation (Figure S12). Upon protonation, the 0→0 vibronic transition of the $S_0 \rightarrow S_1$ electronic transition blue-shifts slightly and the bandwidth narrows, similar to the situation with hydrochloric acid (Figures S13 and S14). However, the structured fluorescent intensity at 541 nm strongly depends on the counterions, decreasing from Cl^- to Br^- and further to I^- (Figures S15−S18). The fluorescence intensity ratio for Cl^-:Br^-:I^- is 57:4:1. Such strong counterion dependence on the fluorescence intensity of the hollow spheres was attributed to the external heavy-atom effect. The origin of the heavy-atom effect was assigned to

the efficient charge transfer between the perylene and halide ions as they came into close contact, forming hydrogen bonds.[12]

In summary, we have demonstrated that protonation of simple pyridyl groups enables new interchromophore interactions such as charge pairing and hydrogen bonding. These new structure-directing forces alter the plate-like assemblies into nanospheric assemblies. Our studies provide a unique paradigm that intermolecular interactions, which result in curvature assemblies, can significantly improve the fluorescent quantum yields of hollow nanospheres when protonated by hydrochloric acid. Considering the easy preparations, we expect that such highly fluorescent hollow nanospheres can be potentially applied to biomedical imaging, drug delivery, and photonic materials.

■ ASSOCIATED CONTENT

Supporting Information. Experiments and calculations, additional spectra, and morphologies. This material is available free of charge via the Internet at http://pubs.acs.org.

■ AUTHOR INFORMATION

Corresponding Author
clzhan@iccas.ac.cn; jnyao@iccas.ac.cn; dequan@wsu.edu

■ ACKNOWLEDGMENT

This work was financially supported by NSFC (Nos. 20872145, 20973182, 50903045, and 20803083), the Chinese Academy of Sciences, Projects 973 (2011CB400808 and 2007CB936401) and 863 (2009AA03Z323), the U.S. National Science Foundation (CHE-0805547), and the CAS/SAFEA International Partnership Program for Creative Research Teams.

■ REFERENCES

(1) (a) Zang, L.; Che, Y. K.; Moore, J. S. *Acc. Chem. Res.* **2008**, *41*, 1596–1608. (b) Wasielewski, M. R. *J. Org. Chem.* **2006**, *71*, 5051–5066. (c) Würthner, F. *Chem. Commun.* **2004**, 1564–1579. (d) Zhan, C. L.; Li, A. D. Q. *Curr. Org. Chem.* **2011**, *15*, 1314–1339.

(2) (a) Wang, W.; Li, L.-S.; Helms, G.; Zhou, H.-H.; Li, A. D. Q. *J. Am. Chem. Soc.* **2003**, *125*, 1120–1121. (b) van Herrikhuyzen, J.; Syamakumari, A.; Schenning, A. P. H. J.; Meijer, E. W. *J. Am. Chem. Soc.* **2004**, *126*, 10021–10027. (c) An, Z.; Yu, J.; Jones, S. C.; Barlow, S.; Yoo, S.; Domercq, B.; Prins, P.; Siebbeles, L. D. A.; Kippelen, B.; Marder, S. R. *Adv. Mater.* **2005**, *17*, 2580–2583. (d) Balakrishnan, K.; Datar, A.; Naddo, T.; Huang, J.; Oitker, R.; Yen, M.; Zhao, J.; Zang, L. *J. Am. Chem. Soc.* **2006**, *128*, 7390–7398. (e) Wicklein, A.; Lang, A.; Muth, M.; Thelakkat, M. *J. Am. Chem. Soc.* **2009**, *131*, 14442–14453.

(3) (a) Van Nostrum, C. F.; Nolte, R. J. M. *Chem. Commun.* **1996**, 2385–2392. (b) Takahashi, R.; Kobuke, Y. *J. Am. Chem. Soc.* **2003**, *125*, 2372–2373. (c) Yamaguchi, T.; Kimura, T.; Matsuda, H.; Aida, T. *Angew. Chem.* **2004**, *116*, 6510–6515. (d) Drain, C. M.; Goldberg, I.; Sylvain, I.; Falber, A. *Top. Curr. Chem.* **2005**, *245*, 55–88. (e) Wang, Z.; Ho, K. J.; Medforth, C. J.; Shelnutt, J. A. *Adv. Mater.* **2006**, *18*, 2557–2560. (f) Elemans, J. A. A.W.; van Hameren, R.; Nolte, R. J. M.; Rowan, A. E. *Adv. Mater.* **2006**, *18*, 1251–1266. (g) Li, W.-S.; Aida, T. *Chem. Rev.* **2009**, *109*, 6047–6076. (h) Wang, Z.; Medforth, C. J.; Shelnutt, J. A. *J. Am. Chem. Soc.* **2004**, *126*, 15954–15955. (i) Wang, Z.; Ho, K. J.; Medforth, C. J.; Shelnutt, J. A. *Adv. Mater.* **2006**, *18*, 2557–2560. (j) Drain, C. M.; Varotto, A.; Radivojevic, I. *Chem. Rev.* **2009**, *109*, 1630–1658.

(4) (a) Yan, X. H.; He, Q.; Wang, K. W.; Duan, L.; Cui, Y.; Li, J. B. *Angew. Chem.* **2007**, *119*, 2483–2486. (b) Yan, X.; Cui, Y.; He, Q.; Wang, K.; Li, J.; Mu, W.; Wang, B.; Ou-yang, Z. *Chem.—Eur. J.* **2008**, *14*, 5974–5980. (c) Wang, C.; Yin, S.; Chen, S.; Xu, H.; Wang, Z.; Zhang, X. *Angew. Chem., Int. Ed.* **2008**, *47*, 9049. (d) Lim, Y. B.; Moon, K. S.; Lee, M. *Chem. Soc. Rev.* **2009**, *38*, 925–934. (e) Ke, D.; Zhan, C.; Li, A. D. Q.; Yao, J. *Angew. Chem., Int. Ed.* **2011**, *50*, 3715–3719.

(5) (a) Huang, C.; Wen, L.; Liu, H.; Li, Y.; Liu, X.; Yuan, M.; Zhai, J.; Jiang, L.; Zhu, D. *Adv. Mater.* **2009**, *21*, 1721–1725. (b) Li, Y.; Li, X.; Li, Y.; Liu, H.; Wang, S.; Gan, H.; Li, J.; Wang, N.; He, X.; Zhu, D. *Angew. Chem., Int. Ed.* **2006**, *118*, 3721–3725. (c) Lu, G.; Ou, Z.; Jiang, J.; Bian, Y. *Eur. J. Inorg. Chem.* **2010**, 753–757. (d) Zhang, X.; Chen, Z.; Würthner, F. *J. Am. Chem. Soc.* **2007**, *129*, 4886–4887. (e) Lv, W.; Zhang, X.; Lu, J.; Zhang, Y.; Li, X.; Jiang, J. *Eur. J. Inorg. Chem.* **2008**, 4255–4261. (f) Golubkov, G.; Weissman, H.; Shirman, E.; Wolf, S. G.; Pinkas, I.; Rybtchinski, B. *Angew. Chem.* **2009**, *121*, 944–948.

(6) (a) He, X.; Liu, H.; Li, Y.; Wang, S.; Li, Y.; Wang, N.; Xiao, J.; Xu, X.; Zhu, D. *Adv. Mater.* **2005**, *17*, 2811–2815. (b) Han, J. J.; Wang, W.; Li, A. D. Q. *J. Am. Chem. Soc.* **2006**, *128*, 672–673. (c) Qian, H.; Negri, F.; Wang, C.; Wang, Z. *J. Am. Chem. Soc.* **2008**, *130*, 17970–17976. (d) Peneva, K.; Mihov, G.; Nolde, Rocha, F.; S.; Hotta, J.-I.; Braeckmans, K.; Hofkens, J.; Uji-i, H.; Herrmann, A.; Müllen, K. *Angew. Chem., Int. Ed.* **2008**, *47*, 3372–3375. (e) Zhang, R.; Wang, Z.; Wu, Y.; Fu, H.; Yao, J. *Org. Lett.* **2008**, *10*, 3065–3068. (f) Huang, J.; Wu, Y.; Fu, H.; Zhan, X.; Yao, J.; Barlow, S.; Marder, S. R. *J. Phys. Chem. A* **2009**, *113*, 5039–5046. (g) Wang, J.; Kulago, A.; Browne, W. R.; Feringa, B. L. *J. Am. Chem. Soc.* **2010**, *132*, 4191–4196.

(7) Wang, K.-L.; Liou, W.-T.; Liaw, D.-J.; Chen, W.-T. *Dyes Pigm.* **2008**, *78*, 93–100.

(8) (a) Lee, C. T.; Yang, W. T.; Parr, R. G. *Phys. Rev. B* **1988**, *37*, 785–789. (b) Becke, A. D. *J. Chem. Phys.* **1993**, *98*, 5648–5652.

(9) (a) Tian, Z.; Shallerz, A. D.; Li, A. D. Q. *Chem. Commun.* **2009**, 180–182. (b) Giaimo, J. M.; Gusev, A. V.; Wasielewski, M. R. *J. Am. Chem. Soc.* **2002**, *124*, 8530–8531.

(10) Herrmann, A.; Weil, T.; Sinigersky, V.; Wiesler, U.-M.; Vosch, T.; Hofkens, J.; De Schryver, F. C.; Müllen, K. *Chem.—Eur. J.* **2001**, *7*, 4844–4853.

(11) (a) Goffman, M.; Harrington, G. W. *J. Phys. Chem.* **1963**, *67*, 1877–1880. (b) Glazunov, V. P.; Odinokov, S. E. *Spectrochim. Acta* **1982**, *38A*, 399–408. (c) Dega-Szafran, Z.; Katrusiakm, A.; Szafran, M. *J. Mol. Struct.* **2001**, *570*, 165–174.

(12) (a) Perrin, F. *J. Phys. Radium* **1926**, *7*, 390–401. (b) Perrin, F. *J. Chim. Phys.* **1928**, *25*, 531–534. (c) Jayaraman, S.; Verkman, A. S. *Biophys. Chem.* **2000**, *85*, 49–57.